The Astrophysical Journal, 618:L67–L70, 2005 January 10

A SCUBA MAP IN THE *SPITZER* FIRST LOOK SURVEY: SOURCE CATALOG AND NUMBER COUNTS

Marcin Sawicki[1] and T. M. A. Webb[2]

Received 2004 January 19; accepted 2004 December 6; published 2004 December 13

ABSTRACT

Using the Submillimetre Common-User Bolometer Array (SCUBA) instrument on the James Clerk Maxwell Telescope, we have made a submillimeter mosaic at 850 μm of a subarea of the *Spitzer* First Look Survey (FLS). Our image covers the central 151 arcmin^2 of the northern extragalactic continuous viewing zone field of the FLS to a median 3 σ depth of 8.4 mJy. The image contains six 850 μm sources detected at 3.0 σ or higher significance. We make the catalog of these SCUBA-selected FLS sources available to the community. After correcting for incompleteness and flux bias, we find that the density of sources brighter than 7 mJy in our field is $2.2^{+2.5}_{-1.0} \times 10^2$ deg^{-2} (95% Poisson confidence limits), which is consistent with other surveys that probe the bright end of the submillimeter population.

Subject headings: catalogs — cosmology: observations — galaxies: formation — galaxies: starburst — galaxies: statistics — infrared: galaxies

1. INTRODUCTION

Launched in the second half of 2003, the *Spitzer Space Telescope* (formerly *SIRTF*), the fourth and final of NASA's Great Observatories, holds the promise of addressing many outstanding questions related to dust-enshrouded galaxy formation at high redshift. One of the first science observations to be undertaken by *Spitzer* is the *Spitzer* First Look Survey (FLS), a first look at the mid-IR sky at sensitivities that are 2 orders of magnitude deeper than previous large-area surveys. In addition to *Spitzer* data at 3.6, 4.5, 5.8, 8.0, 24, 70, and 160 μm, the FLS has also been observed in deep ground-based campaigns at optical (KPNO 4 m to $R = 25.5$, 5 σ in a 2″ aperture) and radio (Very Large Array [VLA] to 115 μJy, 5 σ, per 5″ beam at 1.4 GHz; Condon et al. 2003) wavelengths.[3] The public *Spitzer* FLS data, together with the deep ancillary ground-based observations, will provide the community with the first systematic look at the properties of faint *Spitzer*-selected extragalactic sources.

While *Spitzer* will discover many dust-enshrouded high-z objects and will greatly help us understand their nature, the fact that it does not image at wavelengths longward of 160 μm presents some important limitations. For example, for typical dust temperatures (20–40 K; e.g., Dunne et al. 2000), the longest *Spitzer* passband barely probes longward of the peak of the thermal dust emission for galaxies at even moderate redshifts, making it difficult to estimate their bolometric luminosities and hence infer quantities such as dust masses and star formation rates. Moreover, with increasing redshift (or decreasing dust temperature), an object's dust emission peak shifts redward of the longest *Spitzer* wavelength, causing strong negative k-corrections and making a galaxy at high redshift (or one with low dust temperatures) fade rapidly out of a *Spitzer*-selected sample.

In this Letter, we present complementary long-wavelength imaging observations of a section of the *Spitzer* FLS, obtained at 850 μm with the Submillimetre Common-User Bolometer Array (SCUBA) on the James Clerk Maxwell Telescope (JCMT). In a future paper, we will discuss in detail the multiwavelength properties of sources in the area of our SCUBA map; the purpose of the present Letter is to quickly make available to the community the source catalog of objects from our SCUBA observations within the public-release *Spitzer* FLS.

2. DATA

2.1. *Observations*

We used the SCUBA instrument (Holland et al. 1999) on the JCMT to observe a contiguous area of 151 arcmin^2 centered on the nominal center of the FLS northern extragalactic continuous viewing zone (CVZ) field at R.A. = $17^{\rm h}18^{\rm m}00^{\rm s}$, decl. = $+52°24'30''$ (J2000.0). SCUBA is an array of 37 bolometers at 850 μm and 91 at 450 μm that is able to observe simultaneously at both wavelengths, although particularly excellent weather is required for 450 μm observations. In its jiggle-map mode—which is the mode we used—a SCUBA observation has a footprint of ∼2′ diameter; to cover a large contiguous area, we tiled our field in a spiral pattern on a hexagonal grid, starting at the nominal central FLS coordinates. A typical point in our combined map received a total of 2048 s of integration, split into four visits that were separated in time by many hours and, often, nights.

The data were obtained during 13 nights from 2002 March through 2003 March, using a total of 7.5 usable (out of 10 allocated) shifts of JCMT time. The weather varied from grade 1 to grade 4, or $\tau_{850} \sim 0.1$ to $\tau_{850} \sim 0.45$, where τ_{850} is a measure of the optical depth at 850 μm. To remove the rapidly varying submillimeter sky, we used the standard SCUBA chopping technique with a chop throw of 30″ held constant in right ascension. This technique produces the familiar negative-positive-negative beam pattern apparent in many SCUBA maps and can be used to increase the significance of detection for individual sources by taking advantage of the signal in the off-beams.

Throughout the observing campaign, sky opacity was measured using sky-dip observations every ∼1.5 hr, although less often in exceptionally transparent and stable weather. Pointing checks were performed every 1.5 hr, and the data were flux-calibrated using standard JCMT flux calibrators.

2.2. *Data Reduction*

After removing the nod, the data were flat-fielded and corrected for sky opacity using the sky-dip measurements. The

[1] Dominion Astrophysical Observatory, Herzberg Institute of Astrophysics, National Research Council, 5071 West Saanich Road, Victoria, BC V9E 2E7, Canada; marcin.sawicki@nrc.gc.ca.

[2] Sterrewacht Leiden, Niels Bohrweg 2, Leiden NL-2333 CA, Netherlands; webb@strw.leidenuniv.nl.

[3] See http://ssc.spitzer.caltech.edu/fls.

noise analysis and source detection was complicated by the presence of a strong correlated noise signal (C. Borys 2004, private communication) in the data that affected between one-third and two-thirds of the bolometers at any given time. This nature and cause of the signal is under investigation by the JCMT, but we note that much of the SCUBA data (not just ours) taken during 2002–2003 may suffer from this problem. We attempted to remove the noise in the following way. After the standard flat-fielding and extinction corrections, noise-corrupted bolometers were identified through the presence of strong power in their Fourier spectrum at a characteristic scale of 1/16. Residual sky flux was removed from all the bolometers in the array by subtracting the median sky level at each second, with the sky level determined using only the noncorrupted bolometers. Because the noise on the remaining corrupted bolometers was correlated, it was possible to reduce its effect through the subtraction of the correlated signal. We note that a simple median subtraction did not result in any measurable reduction of the noise, so we used a more sophisticated multiple linear regression technique. The expected noise signal for each corrupted bolometer was estimated using the correlation between all other corrupted bolometers and then removed. As a final step, noise spikes at greater than 3 σ were iteratively removed from the array. The data were then rebinned onto the sky plane to produce a map.

The removal of the correlated noise signal has had three main effects on the final map, as compared to a map produced in the standard way without noise removal. First, it has resulted in an overall decrease in the noise level of ∼15%. Second, it has removed a number of detections from the noncorrected map that do not simply decrease in significance but disappear entirely. Thus, for shallow maps in particular, the presence of the correlated noise signal appears to have led to an increased number of spurious sources. Third, it has led to an overall decrease in the flux levels of the significantly detected sources. The correlated noise in the original map, coupled with our detection algorithm, biased the detected flux levels upward, but the reduction of the overall noise has reduced this effect.

To increase the sensitivity to point sources, the unsmoothed map was convolved with a template beam profile that was made from observations of pointlike calibration sources and contains the negative-positive-negative beam pattern. This technique reduces the frequency of spurious sources that do not convolve well with the beam and increases the signal-to-noise ratio (S/N) by incorporating the flux from the two off-source positions into the final flux measurements. The top panel of Figure 1 shows our beam-convolved map.

We used the method of Eales et al. (2000) to estimate the noise across our map. We produced Monte Carlo simulations of each raw bolometer time stream using the same noise level as in the real data but adding no signal. These simulated data were then reduced using the same set of steps as the real data resulting in a simulated sky map. We produced 500 such simulated sky maps, and the noise at each pixel in the data map, shown in the middle panel of Figure 1, is taken to be the variance between these 500 simulations at that pixel. The noise level determined by this method agrees well with the noise estimated from the real data map. The median noise value is 2.8 mJy (1 σ), and the spatial distribution of the noise level is quite uniform across the entire field except near its edges.

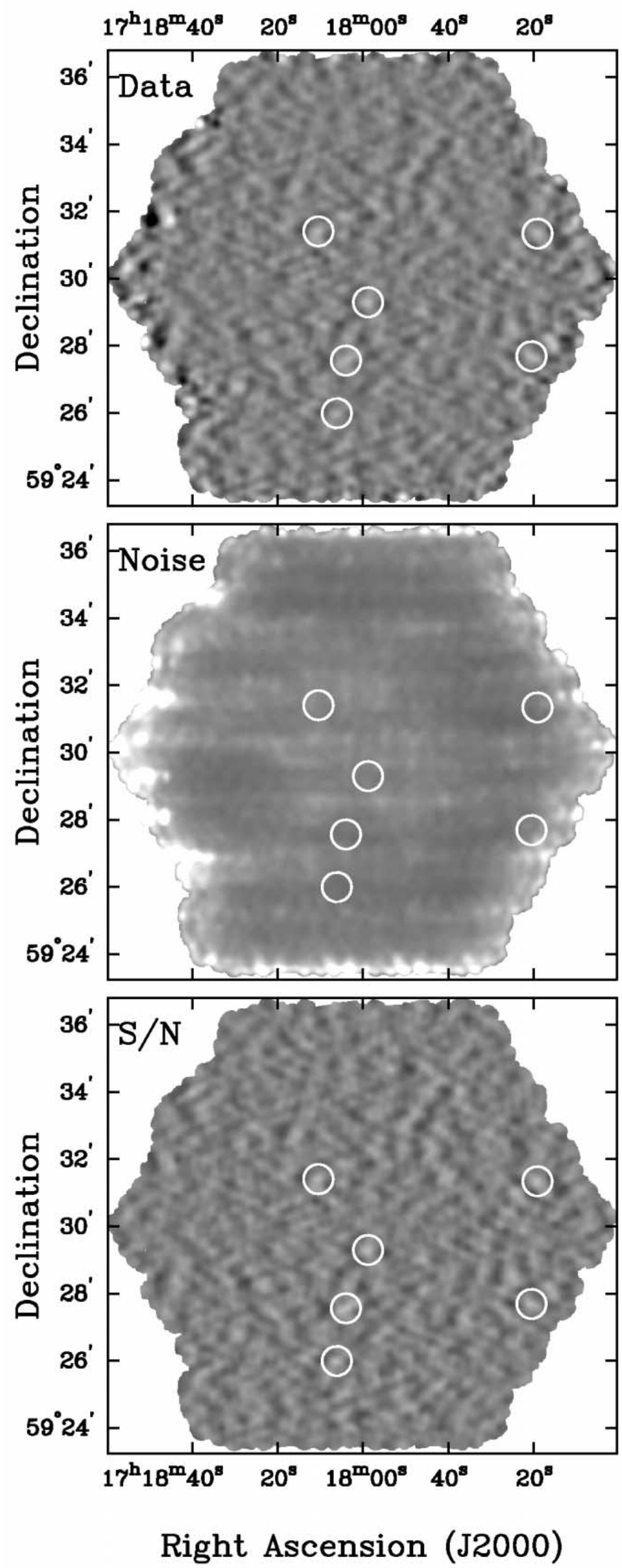

FIG. 1.—Beam-convolved signal (*top*), noise (*middle*), and rms S/N (*bottom*) maps of our 850 μm survey. These maps are mosaics of multiple individual SCUBA pointings. Sources detected at greater than 3.0 σ are marked with circles.

2.3. *Source Detection and Object Catalog*

We used a combination of the data and noise maps to perform an automated source search. An S/N map (Fig. 1, *bottom panel*)

TABLE 1
850 μm SOURCES DETECTED AT GREATER THAN 3.0 σ

Identification (1)	R.A. (J2000.0) (2)	Decl. J2000.0) (3)	$S_{850\ \mu m}$ (mJy) (4)	S/N (5)
FLS 850.1719+3119	17 17 19.1	+59 31 19	8.4 ± 2.5	3.4
FLS 850.1758+2917	17 17 58.9	+59 29 17	9.1 ± 2.7	3.4
FLS 850.1804+2733	17 18 04.2	+59 27 33	7.7 ± 2.3	3.4
FLS 850.1720+2739	17 17 20.6	+59 27 39	8.8 ± 2.7	3.2
FLS 850.1806+2559	17 18 06.4	+59 25 59	7.1 ± 2.2	3.2
FLS 850.1810+3124	17 18 10.6	+59 31 24	8.7 ± 2.9	3.0

NOTE.—Units of right ascension are hours, minutes, and seconds, and units of declination are degrees, arcminutes, and arcseconds.

was produced by dividing the beam-convolved data map by the beam-convolved noise map; all peaks with S/N ≥ 3.0 in this S/N map are source candidates. To make the source-finding procedure objective and automated (a must for our completeness simulations in § 3), the actual search is performed using the SExtractor source-detection software (Bertin & Arnouts 1996) on a truncated version of the S/N map. Specifically, to restrict SExtractor to peaks with S/N ≥ 2.5 and to suppress confusion due to the negative off-beams of bright sources, we set all values S/N < 2.5 to zero before running SExtractor. As confirmed by visual inspection, this technique reliably finds all the peaks above S/N > 2.5. Of 20 peaks with S/N > 2.5, there are six with S/N > 3.

Table 1 presents all sources detected with S/N > 3. Column (1) gives the source identification, columns (2) and (3) give the coordinates of the source determined by SExtractor in the truncated S/N map, column (4) gives the source flux, and column (5) lists the significance of the detection. However, we caution the reader that some of our sources may not be real but may be statistical noise fluctuations in the data.

3. SOURCE COUNTS

To date, two surveys have targeted the bright end ($S_{850\ \mu m} \gtrsim 10$ mJy) of the submillimeter population, and both show a steep slope of the cumulative source counts. Scott et al. (2002) surveyed two spatially independent fields with a total area of 260 arcmin^2, while Borys et al. (2002, 2003) studied an area of 165 arcmin^2 in the region of the northern Hubble Deep Field. Both surveys show strong qualitative clustering of sources, which may skew their source count results. Here we use our 151 arcmin^2 FLS SCUBA map to make a third, independent measurement of the submillimeter source counts at the bright end of the population.

Our *raw* cumulative source counts are presented in column (3) of Table 2, where we have counted all objects *detected* at S/N ≥ 3.0. However, we are interested in sources that are close to the noise level, and so, to properly calculate the source density, we must account for two effects: incompleteness and flux bias. Clearly, the number counts of faint sources near the detection threshold will suffer from incompleteness, making it necessary to correct their observed numbers upward. In addition, however, detected sources will also have suffered from flux boosting: while sources whose flux densities are scattered below the detection threshold are not counted in the sample, those that are scattered into the sample from below the detection threshold will necessarily have their flux densities overestimated. These two effects compete against each other, but for a source population where numbers increase quickly with decreasing true flux density (as is the case here), flux boosting should dominate.

We studied these issues using Monte Carlo simulations that implant artificial sources into our data and seek to recover them

TABLE 2
850 μm NUMBER COUNTS IN THE *SPITZER* FLS

$S_{850\ \mu m}$ (mJy) (1)	$n_{\rm objects}$ (2)	Raw $N(>S)$ (3)	Corrected $N(>S)$ (4)
7	6	143^{+168}_{-64}	216^{+254}_{-97}
8	4	95^{+148}_{-69}	108^{+168}_{-78}
9	1	24^{+109}_{-23}	23^{+105}_{-22}

using the same technique that we used for constructing our source catalog in § 2.3. We generated artificial sources by flux-scaling the empirical beam map constructed from observations of bright point-source flux calibrators. An artificial source was then added at a random (but known) location to the data map, the resulting map was divided by the noise map to form the S/N map, and then the object-finding and flux measurement procedures used on the real data were applied to search for the artificial object. To statistically assess the completeness and flux bias properties of our map, this procedure was repeated, one artificial object at a time, for a range of input fluxes and spatial positions.

This Monte Carlo procedure applied to our SCUBA map results in a matrix, $S_{\rm true,\,obs}$, that gives the probability that, for a source of a known input flux density $S_{\rm true}$, we will recover an object of an observed flux density $S_{\rm obs}$. To understand the incompleteness and flux bias effects on the *population* of sources, we need to consider their effects on a plausible true source count distribution. Following Borys et al. (2003), we assume the following functional form to describe the underlying source count population:

$$\frac{dN(>S)}{dS} \propto \left[\left(\frac{S}{S_0}\right)^{\alpha} + \left(\frac{S}{S_0}\right)^{\beta}\right]^{-1}; \qquad (1)$$

we adopt $S_0 = 1.8$ mJy, $\alpha = 1$, $\beta = 3.3$ (Scott et al. 2002), although varying these parameters within reasonable ranges ($S_0 = 0.5$–5, $\alpha = 0.5$–2, $\beta = 2$–4) does not drastically affect our results. We then multiply the assumed source count model of equation (1) by the transform matrix $S_{\rm true,\,obs}$ to obtain the "observed" source counts. The ratios of the integrated source counts in the underlying source count model to those "observed" by our procedure, give us the correction factors that need to be applied to the raw source counts in Table 2 to correct for incompleteness and flux bias.

The corrected integrated source counts are given in column (4) of Table 2 and are plotted in Figure 2 together with counts from other surveys. Our 850 μm FLS source counts are clearly in agreement with both the results of the 8 mJy survey of Scott et al. (2002) and with the Hubble Deep Field data of Borys et al. (2003), and we conclude that, at least on the basis of source number densities, there is no evidence that our FLS subfield is not representative of the submillimeter galaxy population.

4. SUMMARY AND DISCUSSION

In this Letter, we presented our SCUBA observations of a 151 arcmin^2 subarea in the northern CVZ field of the *Spitzer* FLS. We found a total of six sources at S/N ≥ 3.0 and make their particulars available to the community. Our integrated source counts are consistent with those of the other two surveys of the bright end of the submillimeter population, namely, the 8 mJy survey (Scott et al. 2002) and the Hubble Deep Field supermap (Borys et al. 2002, 2003). Given that extragalactic submillimeter sources cluster strongly on the scales of current

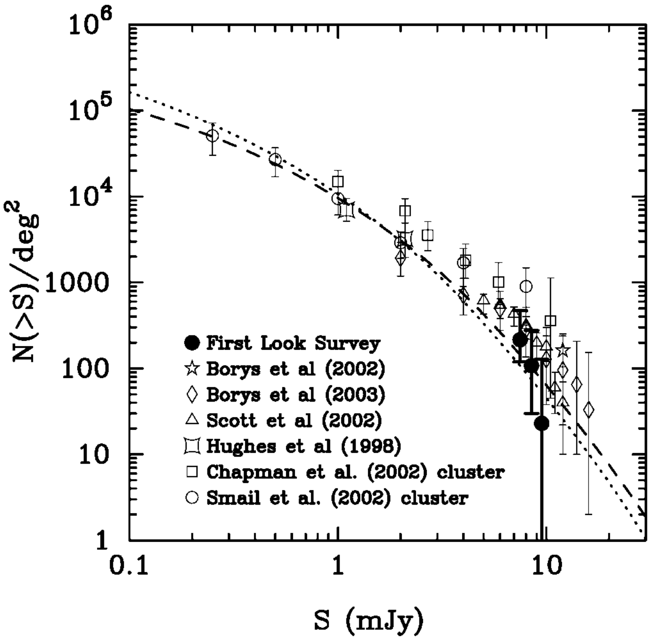

FIG. 2.—Cumulative 850 μm number counts. The filled circles show the results from the present work in the *Spitzer* FLS, and results are also shown from Borys et al. (2002, 2003), Scott et al. (2002), Hughes et al. (1998), Chapman et al. (2002), and Smail et al. (2002). Error bars are 95% Poisson confidence limits. Following Borys et al. (2003), overlaid are two predictions based on representative galaxy evolution models from Rowan-Robinson (2001)—the dashed line is for a universe with $(\Omega_M, \Omega_\Lambda) = (1.0, 0.0)$, and the dotted line is for $(\Omega_M, \Omega_\Lambda) = (0.3, 0.7)$.

surveys, the fact that our number counts agree with those of the other two surveys gives an important confirmation of the numbers of SCUBA sources at the bright end of the population. Equally significantly, the agreement between our number counts and those of other surveys suggests that the subfield of the FLS that we imaged is not unrepresentative of the extragalactic sky.

We will study the multiwavelength properties of the submillimeter sources in our map in future work. In the meantime, we have compared the positions of our SCUBA detections with those of objects in the 1.4 GHz VLA map of the FLS (Condon et al. 2003) and found no correspondence between the radio-selected and the submillimeter-selected populations down to the limit of the VLA catalog (115 mJy, 5 σ). This lack of radio detection of any of our submillimeter sources can be used to constrain their redshifts (Dunne et al. 2000; see also Yun & Carilli 2002): given the VLA flux limit and the rather narrow dynamic range of these data, most of our submillimeter sources appear to be at $z \gtrsim 1.6$–1.7 (however, these results are likely to be affected by flux boosting). These redshift constraints are in line with our current knowledge of the redshift distribution of submillimeter-selected sources: the median redshift of the population is believed to lie at $z \sim 2$–3, and evidence exists of a flux-redshift relation, such that more luminous submillimeter-selected systems (such as those in our survey) reside at higher redshifts than the less luminous objects (Ivison et al. 2002; Smail et al. 2002; Webb et al. 2003; Chapman et al. 2003; Clements et al. 2004). The lack of 1.4 GHz detection of our submillimeter sources is thus not unexpected: deeper radio data will be needed to detect and identify these systems. We will explore these issues in the future.

We thank the Joint Astronomy Centre staff who helped us obtain these data and our colleagues who carried out some of these observations through the Canadian flexible scheduling scheme. We thank Colin Borys for several useful discussions. The JCMT is operated by the Joint Astronomy Centre on behalf of the Particle Physics and Astronomy Research Council of the United Kingdom, the Netherlands Organisation for Scientific Research, and the National Research Council of Canada.

REFERENCES

Bertin, E., & Arnouts, S. 1996, A&AS, 117, 393
Borys, C., Chapman, S. C., Halpern, M., & Scott, D. 2002, MNRAS, 330, L63
———. 2003, MNRAS, 344, 385
Chapman, S. C., Blain, A. W., Ivison, R. J., & Smail, I. R. 2003, Nature, 422, 695
Chapman, S. C., Scott, D., Borys, C., & Fahlman, G. 2002, MNRAS, 330, 92
Clements, D. L., et al. 2004, MNRAS, 351, 447
Condon, J. J., et al. 2003, AJ, 125, 2411
Dunne, L., Eales, S., Edmunds, M., Ivison, R. J., Alexander, P., & Clements, D. L. 2000, MNRAS, 315, 115
Eales, S., Lilly, S. J., Webb, T. M. A., Dunne, L., Gear, W., Clements, D. L., & Yun, M. 2000, AJ, 120, 2244
Holland, W. S., et al. 1999, MNRAS, 303, 659
Hughes, D. H., et al. 1998, Nature, 394, 241
Ivison, R. J., et al. 2002, MNRAS, 337, 1
Rowan-Robinson, M. 2001, ApJ, 549, 745
Scott, S. E., et al. 2002, MNRAS, 331, 817
Smail, I., Ivison, R. J., Blain, A. W., & Kneib, J.-P. 2002, MNRAS, 331, 495
Webb, T. M. A., Lilly, S. J., Clements, D. L., Eales, S., Yun, M., Brodwin, M., Dunne, L., & Gear, W. K. 2003, ApJ, 597, 680
Yun, M. S., & Carilli, C. L. 2002, ApJ, 568, 88